ELSEVIER

Cement & Concrete Composites 22 (2000) 281–291

Cement & Concrete Composites

www.elsevier.com/locate/cemconcomp

Experimental programme and analytical study of bond stress distributions on a composite plate bonded to a reinforced concrete beam

E.E. Etman, A.W. Beeby *

School of Civil Engineering, University of Leeds, Leeds LS2 9JT, UK

Abstract

An experimental investigation of the bond stress along the concrete–epoxy–plate interface is presented. The main variables were the plate end cut-off and the different corrosion ratios induced to the lower reinforcement of the beams. This was supported with a parametric study for several variables based on a simplified model. The results showed that the plate breadth to thickness ratio, (b_{pl}/t_{pl}), was a very significant factor, which affects the bond stress concentration at the plate end. It was also found that the plate end cut-off may affect the bond stress concentration. However, more investigation is still needed to address this issue. © 2000 Elsevier Science Ltd. All rights reserved.

Keywords: Interfacial bond stresses; FRP; Repair; Strengthening; Corroded reinforcement; Reinforced concrete beam; Stress concentration; Plate end geometry

1. Introduction

The technique of bonding steel plates to concrete beams using epoxy adhesives has been used in the UK to strengthen a number of trunk road bridge structures and has proved to be successful over three decades. Although the technique has been recognized to be an effective and convenient method of improving the structural performance of members under load, the use of steel plates has its disadvantages including difficulties in preparing, transporting and handling the plates, the amount of site work involved and the possibility of corrosion that could adversely affect the bond strength. For these reasons, Fiber reinforced polymer (FRP) plates are being considered as a means of overcoming these shortcomings.

In this study a series of reinforced concrete beams were plated with carbon fiber reinforced polymer (CFRP) plates. The bond stress distribution was investigated and a parametric study was conducted. The work described in this paper formed part of the investigation carried out as a Ph.D. student by the first author. It is presented more fully in (1).

* Corresponding author. Fax: +44-0-113-2332304.
E-mail address: a.w.beeby@leeds.ac.uk (A.W. Beeby).

2. Previous work

Plated beams generally fail in a brittle manner characterised by either sudden interface bond failure or a horizontal failure in the concrete parallel to the plate. The interfacial bond stress and normal stress concentration near to plate ends are considered to be the main factors leading to this failure.

Attempts to determine the distribution of the shear and direct stresses near the plate ends have taken the form of analytical studies, finite element analysis, small-scale concrete-adhesive-plate joint testing and large-scale beam testing. Swamy et al. [2], related the ultimate bond stress to the concrete cube strength, claiming that the bond stress varied from 6.0 to 8.3 N/mm^2 for cube strengths 25–70 N/mm^2. Ranisch and Rostasy [3] also related the bond stress to compressive strength; the bond stress was 8 N/mm^2 for cube strength of 30 N/mm^2, a higher value for comparable cube strength than Swamy et al. [2]. Swamy et al. [4], in another attempt related the bond stress to the concrete tensile strength. It was found that the maximum bond stress was equal to $\sqrt{2}\times$ tensile strength of the concrete. As the concrete tensile strength is unlikely to exceed 4–5 N/mm^2 for normal strength mixes, this would give a maximum bond stress of 6–7 N/mm^2. Swamy et al. [4]

0958-9465/00/$ - see front matter
PII: S0958-9465(00)00030-5

also conclude that the peak interfacial bond stress determined experimentally had a value of 2τ, where τ is the elastic shear stress. This result contradicted a previous result by Jones et al. [5] who found that the peak bond stress determined experimentally had no consistent relationship with the elastic shear stress τ. Roberts [6] concluded that the failure of epoxy bonded steel plates was likely to occur at bond stresses between 3 and 5 N/mm^2, combined with normal stresses between 1 and 2 N/mm^2, although these limits depended on the strength of the epoxy adhesive and the adjacent concrete layer and on the method of surface preparation.

Chajes et al. [7], conducted single lap shear tests to study the bond strength, surface preparation and concrete strength. They concluded that the surface preparation could affect the bond strength. They also concluded that, where the failure mode of the joint was governed by shearing the concrete directly beneath the adhesive, the value of the ultimate bond strength was proportional to $\sqrt{f'_c}$.

Quantrill et al. [8], Chajes et al. [7], Roberts [6] and Malek et al. [9] all conducted extensive experimental and analytical studies of the stress concentration at the plate ends. Malek et al. [9] introduced an analytical note that combined the ideas of the previous work and has done additional mathematical work to establish the stresses at the plate end.

3. Experimental

Preliminary studies of the literature suggested that there was insufficient information available on the effect of bonding CFRP plates to reinforced concrete beams. Since a principal use of bonded plates is to repair beams, where the reinforcement has suffered from corrosion, it seemed especially valuable to study this situation directly. A further variable which initial consideration suggested might be significant but which had not been covered extensively by other researchers was the shape of the end of the plate. A tapered end might, for example, reduce the stresses developed in the concrete in the region of the plate end.

An experimental program was planned and carried out to investigate the behavior of the bond stress over the bonded CFRP plate. The tests were carried out using small repaired beam specimens as shown in Fig. 1. The beams were of a rectangular cross-section, 125 mm wide, 150 mm deep, and 1320 mm long. They were tested under four point bending over a simple span of 1200 mm. All beams were reinforced in tension with two 12 mm diameter ribbed bars of high tensile steel. Two 8 mm diameter mild steel bars were used as top steel. 8 mm diameter mild steel links were incorporated to guarantee that none of the beams would fail in shear. Links were

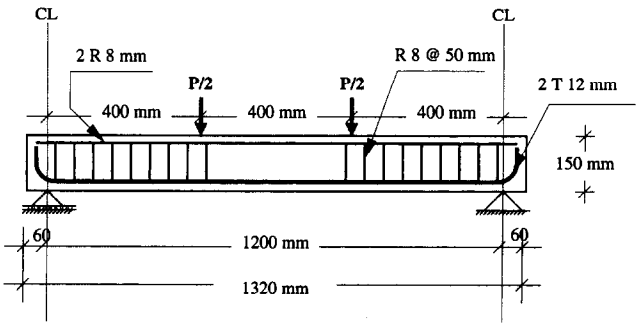

Fig. 1. Details of reinforced concrete test beams.

spaced at 50 mm over the shear spans, while no shear reinforcement was provided in the constant moment region.

The CFRP plates used in this research were 1.3 mm thick and 50 mm wide and were cut to the required length. Three configurations for the region at the end of the CFRP plates were considered. Fig. 2 shows the plate arrangements used for the beams strengthened with CFRP plates types CF or CF-II. Beams type CF-I had identical plates on the soffit to beams type CF, but were provided with additional plates bonded to the sides of the beams. The rationale behind the introduction of these small plates was that observed failures commonly occurred in the concrete just above the interface between the plate and the beam. It was thought possible that reinforcing this limited zone might lead to significantly improved performance without the application of extensive side plating. The CFRP plates were tested to establish their properties and showed a linearly elastic behavior until sudden failure occurred. Table 1 gives the properties of the CFRP plates.

The effect of corroded reinforcement was studied by testing beams with corroded main reinforcement. In the beams that were to be corroded, the central 500 mm of reinforcement were exposed and corroded by placing the beams in a tank of salt water and then passing an electric current through the system at constant voltage until the required amount of corrosion had taken place. After corrosion, the bars were cleaned by wire brushing and the concrete reinstated. The procedure is explained in detail in Beeby and Etman [10]. Losses of 10%, 15% or 20% of the reinforcement cross-section were achieved. The effect of different plate end details on the stress concentration at the plate curtailments was also investigated. Overall, 16 beams were tested.

The beams were subdivided into four groups according to the plate end geometry and corrosion ratio. The plate geometry and identification system used for the specimens are given in Fig. 2.

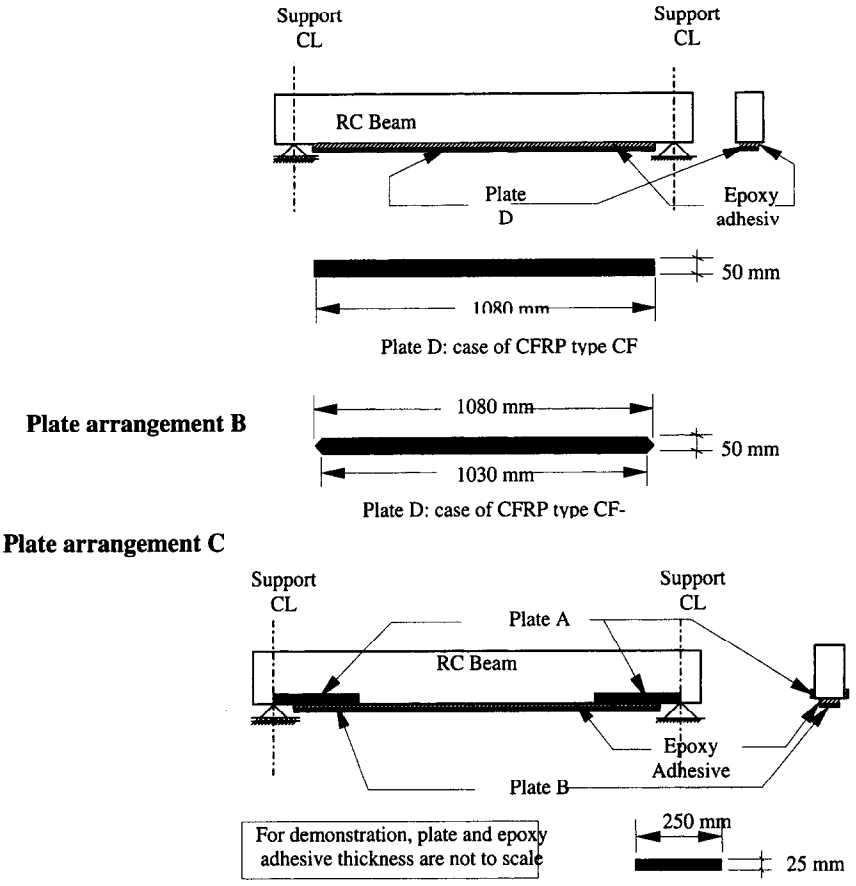

	0% corrosion	10% corrosion	15% corrosion	20% corrosion
No plate	FG1	FG1-10	FG1-15	FG1-20
Plate arrangement A	FG1-CF	RG1-CF-10	RG1-CF-15	RG1-CF-20
Plate arrangement B	FG1-CF-I	RG1-CF-I-10	RG1-CF-I-15	RG1-CF-I-20
Plate arrangement C	FG1-CF-II	RG1-CF-II-10	RG1-CF-II-15	RG1-CF-II-20

Fig. 2. Details of CFRP plates.

3.1. Preparation of reinforced concrete beams

The same concrete mix which achieved an average concrete compressive strength of 62 MPa at 28 days was used for all beams. After casting, the beams were kept over-night in their moulds covered with damp hessian and polyethylene sheets. The formwork was removed the following day and the beams were then cured at 99% relative humidity and 20 ± 2°C for seven days. The beams were then left to cure at room temperature in the laboratory area until they were taken for corroding. After the required amount of corrosion had been achieved, the bars were cleaned and the cut-out area filled with a concrete 'patch repair'. Curing was then continued until the CFRP plates were affixed.

Table 1
Properties of CFRP plates

Properties	Given by manufacturer	Test results
Tensile stress	2400 N/mm^2	2370 N/mm^2
Maximum elongation	1.4%	1.5–1.8%
Modulus of elasticity	150.0 kN/mm^2	154.0 kN/mm^2

3.2. Preparation and bonding of CFRP plates

At a minimum age of 28 days after completion of the repair, and before bonding the CFRP plate to any specimen, the concrete surface was cleaned and roughened using a needling hammer to remove the cement skin and expose the coarse aggregate. The remaining dust and fine concrete particles were removed with high-pressure air. In addition, the CFRP plate was also wiped with a piece of cloth wetted in thinner to remove any carbon dust and then left to dry before bonding.

After cleaning, the strain gauges were attached. Bonding the plates to the beams was done through a layer of a two-component epoxy adhesive (Sika Sikadur-30). The plate was put at once on top of the concrete specimen. A slight pressure was applied to the plate by putting heavy steel plates on top of them. The specimens were tested after a minimum period of seven days to guarantee full curing of the epoxy adhesive. Properties of the epoxy adhesive are given in Table 2.

3.3. Instrumentation and measurements

In this paper, only the instrumentation relevant to the measurement of the bond stress distribution along the plate is considered; this is shown in Fig. 3(a) and (b). Reference may be made to [1] for full details of the instrumentation.

Table 2
Properties of epoxy adhesive

Properties	Given by manufacturer	Test results
Compressive strength	> 100 N/mm^2	70–80 N/mm^2
Adhesive strength to concrete	> 2 N/mm^2	N/A
Elastic modulus	12.8 kN/mm^2	12.5 kN/mm^2
Poisson's ratio	0.3	0.33

Strain gauges were glued on the inner and outer faces of the CFRP plate. For the CFRP plates fixed on the beam sides (plate A), two strain gauges were attached to each of the side plates. The positions of the strain gauges are shown in Fig. 3(a).

To measure the concrete surface strains, strain gauges were fixed on the top surface and on one side of the beam at mid-span. At the beam soffit, strain gauges were glued at intervals along the centerline of the section. These were to give the strain distribution along the beam span for comparison with the strains measured on the CFRP plate. Locations of the strain gauges are shown in Fig. 3(b).

3.4. Test procedure

The load was applied in 2.5 kN increments until the first crack was detected, then, the load increment was increased to 5 kN up to 75% of the expected failure load. At about 75% of the failure load, the increment was reduced to a value between 2 and 1 kN until failure occurred.

4. Test results and discussion

This section presents the bond stress distributions along the plate length. The bond stress is obtained from the differences between the tensile forces at different

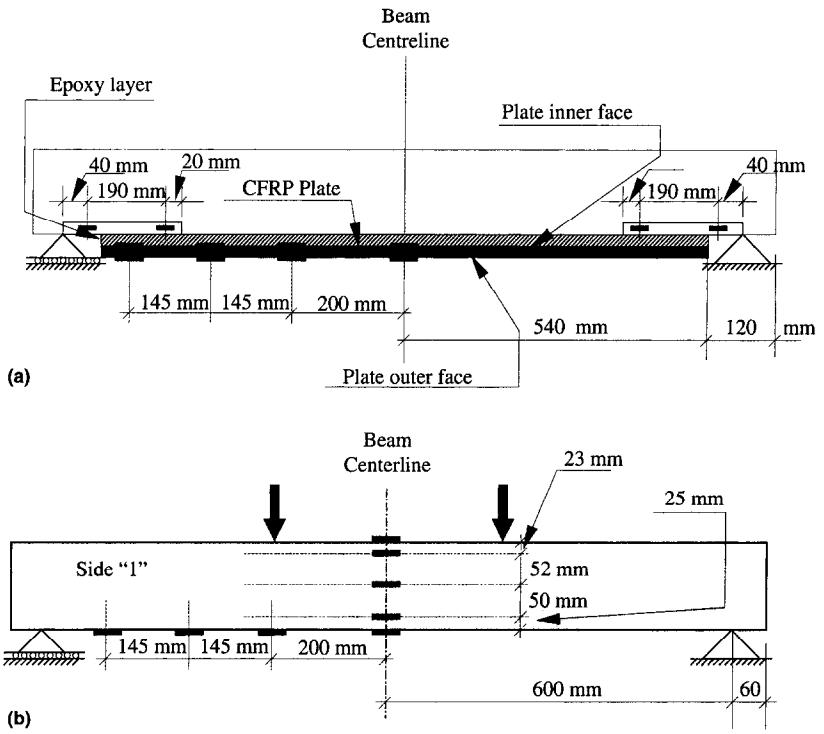

Fig. 3. Instrumentation: (a) location of ERS gauges on CFRP plates; (b) location of ERS gauges on concrete beam.

sections along the plate. It should be noted that this procedure results in an average bond stress over the distance between any two gauges and not the actual stress at any point.

Fig. 4 shows the bond stress distribution for four beams (FG1-CF, RG1-CF-10, RG1-CF-15 and RG1-CF-20). This sample was chosen to show the effect of different corrosion ratios on the behavior of the beams. The bond stress at different positions along the plate at service load of 60 kN is given in Table 3.

The bond stress curves were plotted at different loads up to a level very close to failure. Fig. 5 shows the bond stress distribution for beams RG1-CF-10, RG1-CF-I-10 and RG1-CF-II-10 at three load levels; 20, 60 and 100 kN. A generally similar trend was obtained for all specimens, regardless of the plate details. The rate of change in the bond stresses along the plate, outside the constant moment area, was small until about 60% of the failure load. After this, the rate was higher until 95% or more of the ultimate load beyond which the rate decreased again.

5. Discussion of experimental results

It was observed from the test results that the bond stress, in almost all of the beams, was nearly equal to zero over the constant moment zone, especially at the lower level of loading (see Fig. 5(a)). This was expected at this stage, as the constant moment implies zero shear and hence zero bond stresses. However, with the increase in loading, bond stresses within the constant moment area started to increase noticeably, (see Fig. 5(b) and (c)). With the higher loads, flexural cracks started to appear in the constant moment region which will have resulted in high local bond stresses. Though

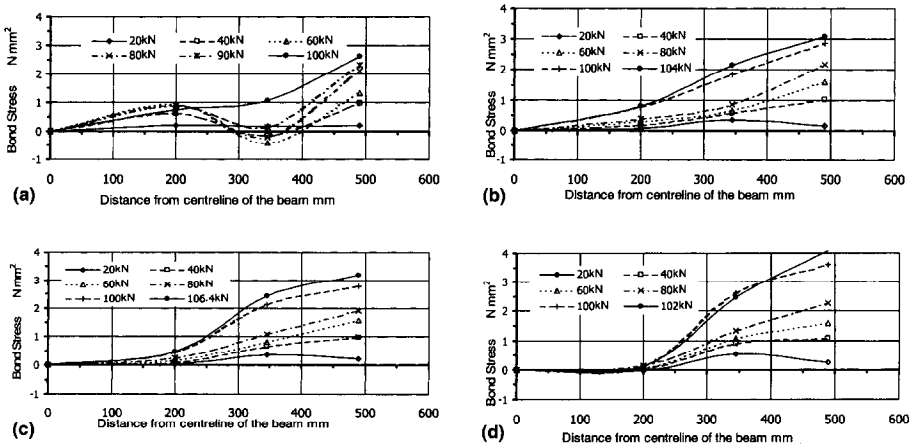

Fig. 4. Measured bond stress distributions for typical beams: (a) beam FG1-CF; (b) beam RG1-CF-10; (c) beam RG1-CF-15; (d) beam RG1-CF-20.

Table 3
Bond stress at different positions along the plate at 60 kN

Specimen	Bond stress at different positions measured from beam centreline (N/mm²)			f_{cu} (N/mm²)		Failure load P_u
	200 mm	345 mm	490 mm	Parent	Repair	kN
FG1-CF	0.92	−0.42	1.32	61.9	N/A	99.8
RG1-CF-10	0.16	0.83	1.58	68.5	79.9	106
RG1-CF-15	0.30	0.66	1.6	66.3	78.4	104.5
RG1-CF-20	0.05	1.07	1.59	67.3	65.3	104.0
FG1-CF-I	0.13	0.88	1.59	67.3	N/A	106
RG1-CF-I-10	0.16	0.77	1.69	63.7	71.9	105
RG1-CF-I-15	0.26	0.96	1.72	68.5	64.7	104.1
RG1-CF-I-20	0.28	1.01	1.67	63.7	64.7	104
RG1-CF-II-10	0.21	0.79	1.41	68.5	79.9	105
RG1-CF-II-15	0.07	0.96	1.48	66.3	78.4	100.1
RG1-CF-II-20	0.15	1.10	1.42	67.3	65.3	101.0

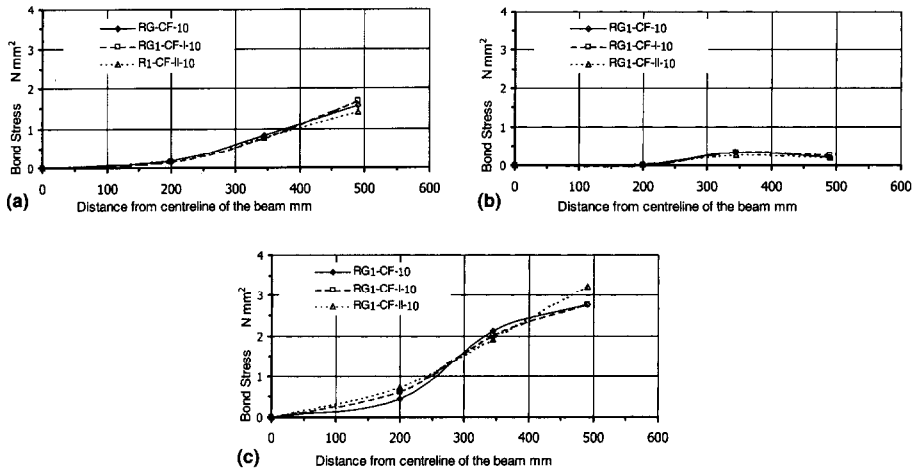

Fig. 5. Measured bond stress distributions at various load levels: (a) load = 20 kN; (b) load = 60 kN; (c) load = 100 kN.

the average bond stress over the whole zone should remain at zero (positive and negative bond stresses on either side of a crack should balance out), local variations of stress in the CFRP plate and the nature of the instrumentation may well result in bond stresses being indicated by the instrumentation.

In the second segment of the curves, the segment covering the parts of the plates adjacent to the constant moment zone, higher bond stresses were recorded. These bond stresses appeared to be roughly proportional to the shear forces on the beam.

In the third segment of the curve, covering the region close to the end of the CFRP plate, significantly higher values of bond stress were observed. The change in the bond stress was very steep at the higher load levels.

The comparison of the bond stresses in the beams strengthened with different types of CFRP plates at different corrosion rates showed that there was no significant change in the bond stress distribution of the beams due to these factors. However, from Table 3, it may be concluded that at service load the bond stress near the plate ends was the highest for beams bonded with CFRP plate type CF-I, while it was the lowest for beams bonded with plates type CF-II. It could thus be concluded that the plate end geometry has had some effect on the bond stress at the plate–epoxy–concrete interface, however, more investigation needs to be conducted to establish this more clearly since the effect is small.

The beams repaired with CFRP plate type CF-I showed higher changes in bond stress due to the change in corrosion level than the beams repaired with the other two types of the plates. It seems here that the side plates improved the internal forces distribution within the composite section allowing higher strains in the plate with the higher corrosion ratio.

Bond stresses at the plate–epoxy–concrete interface may be generated by:

1. Change in moment between sections. These bond stresses will be proportional to shear force on the beam;
2. Local anchorage effects resulting in concentration of bond and normal stresses near the end of the plate; and
3. The formation of cracks. These may result in local high bond stresses similar to those around plate ends and could cause local debonding.

The final resulting stress is a combination of these effects. Fig. 6 shows a schematic drawing of the elements of the bond stresses at the interface. It will be seen that the combination of effects can be expected to produce a very variable distribution of bond stress over the length of the plate. This, together with the averaging inherent in the calculation of the bond stresses, means that the experimental curves are unlikely to be either very consistent or smooth.

6. Theoretical parametric study

In the parametric study conducted here the analytical method developed by Malek et al. [9], has been used. The effect of the plate thickness, the concrete compressive strength, the plate modulus of elasticity, the plate width to thickness ratio and the plate end geometry on the bond stresses at the plate end was investigated. Malek et al.'s analysis does also cover the distribution of stresses resulting from the presence of a flexural crack in the RC beam. This aspect has been ignored in this study.

The model of Malek et al. [9], is based on the assumptions of linear elastic and isotropic behavior of the FRP plate, epoxy, concrete and steel reinforcement.

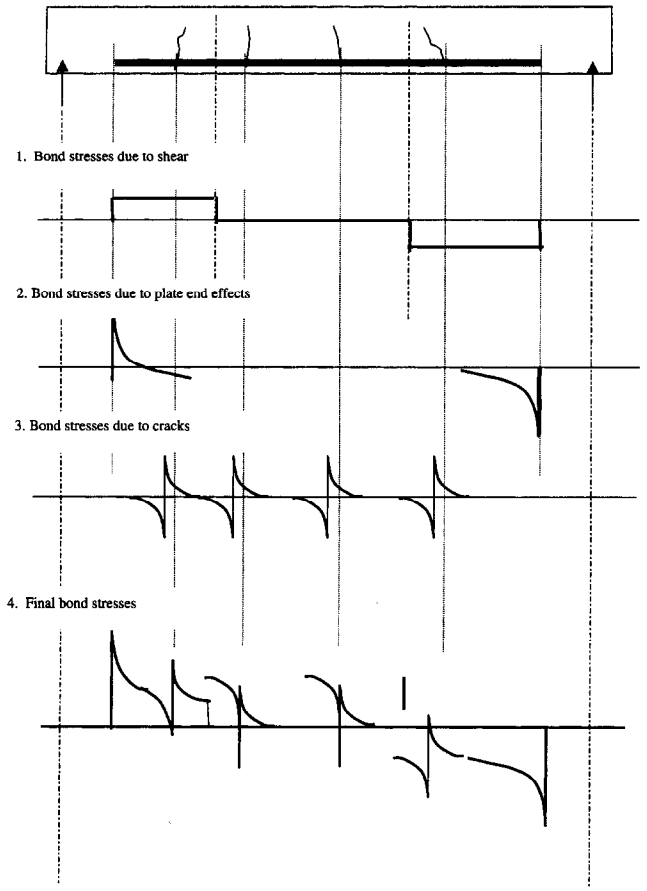

Fig. 6. Factors contributing to the total bond stress.

Also, linear strain distribution through the full depth of the beam section was assumed.

The interfacial bond stress between the plate and epoxy can be calculated by considering the equilibrium of an infinitesimal part of the plate (see Fig. 7).

In the figure, $\tau(x)$ and $f_n(x)$ are the bond and normal stresses, respectively. Only the final equation for $\tau(x)$ is presented here, the full derivation of the equations are given in Ref. [9].

The bond stress can be defined as the change in the axial force in the plate divided by the bonded surface area of the plate over a distance dx. This may be expressed in the following form:

$$\tau(x) = t_{pl}\{b_3 A\cosh(Ax) + b_3 A\sinh(Ax) + 2b_1 x + b_2\}, \tag{1}$$

where:

$$A = \{G_a/(t_a t_{pl} E_p)\}^{0.5}, \qquad b_1 = \frac{\bar{y} a_1 E_p}{E_c I_{tr}},$$

$$b_2 = \frac{\bar{y} E_p}{E_c I_{tr}}(2a_1 L_0 + a_2) \quad \text{and}$$

$$b_3 = E_p\left(\frac{\bar{y}}{E_c I_{tr}}(a_1 L_0^2 + a_2 L_0 + a_3) + 2b_1 \frac{t_a t_{pl}}{G_a}\right).$$

The maximum bond stress, τ_{max}, occurs at the cut-off end of the plate and an expression can be obtained for this by substituting the value of x to equal zero in Eq. (1), giving:

$$\tau_{max} = t_{pl}(b_3 A + b_2), \tag{2}$$

where the bending moment at any point may be expressed as follows:

$$M(x_0) = a_1 x_0^2 + a_2 x + a_3,$$

where a_1, a_2 and a_3 are constants.

The origin of x_0 is arbitrary and can be assumed at any suitable point at a distance L_0 from the plate cut-off end. And could be expressed as:

$$x_0 = x + L_0.$$

G_a is the shear modulus of elasticity of the adhesive layer; t_{pl} is thickness of the plate; t_a the thickness of the epoxy adhesive layer; I_{tr} the moment of inertia of the transformed section based on concrete; $\bar{y}$ the distance from neutral axis of the strengthened section to the centre of the plate; L_0 the distance from the plate end cut-off; E_p the plate modulus of elasticity; E_c is the concrete modulus of elasticity.

The predictions of the method will be compared firstly with the experimental results and then a parametric study will follow to illustrate the effect of some factors thought to affect the interfacial stresses.

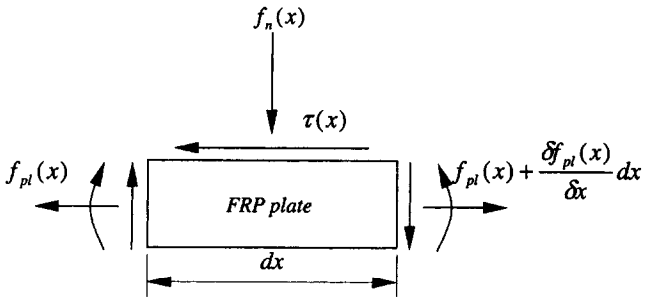

Fig. 7. Stresses on a small element of plate.

6.1. Comparison with experimental results

In Fig. 8 comparisons between the analytical model and the experimental results from beams FG1-CF and FG1-CF-I are presented.

The experimental results do not fit the analytical results well, though the general magnitudes are similar. It should be noted that, while the theoretical approach gives the shear stress at a point, the experimental values are the average stress over the length between two gauge points. Furthermore, as noted earlier, the analysis used does not account for the effects of flexural cracking

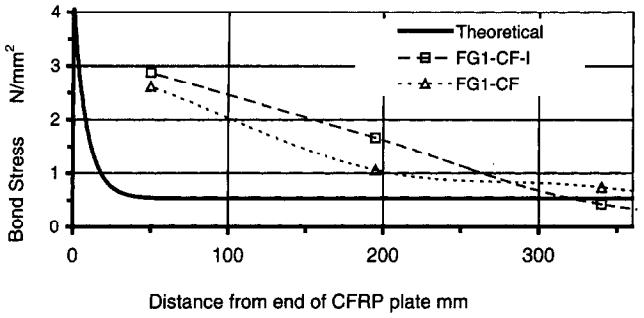

Fig. 8. Comparison of measured and calculated bond stresses.

which will result in local distortions to the measured strains and hence to the inferred bond stresses. It is therefore not unexpected if the direct agreement between the calculated and measured results is not particularly good. Both analytical and experimental results do, however, show high bond stresses near the end of the plate.

6.2. Effect of different variables on the plate end stresses

This section describes the results of a parametric study to investigate the effect of plate thickness, concrete strength, plate modulus of elasticity, plate width to thickness ratio (i.e. changing the plate width while keeping the same plate cross-sectional area), and the plate end geometry. While investigating a variable, the other variables were kept constant at the experimental base values. These were; 1.3 mm plate thickness, 62 N/mm^2 concrete strength, 150 kN/mm^2 plate modulus of elasticity, 38 for plate width to thickness ratio and square ended plate for the plate geometry. Poisson's ratio for the adhesive was taken 0.33 for the whole investigation.

6.3. Effect of plate thickness

Three thickness were investigated; 0.65, 0.95 and 1.3 mm. It can be seen from Fig. 9(a) that the thicker the plate the higher is the bond stress at the interface. At the plate ends, the 0.95 and 0.65 mm thick plates showed 16% and 31%, respectively, lower bond stress than the 1.3 mm thick plate. This result is to be expected since the stresses would be expected to increase with increase in plate stiffness. It should be noted that the process of producing plates of different thicknesses is likely to influence the properties of the plates. This has not been taken into account here.

6.4. Effect of concrete strength

A comparison between the bond stress distribution as a function of the concrete strength is shown in Fig. 9(b). The concrete strengths investigated were: 30, 45 and 62 N/mm^2. It can be seen that the concrete strength does not have a significant effect on the interface stresses.

6.5. Effect of the modulus of elasticity of the plate

An investigation for plates with three different moduli of elasticity is shown in Fig. 9(c) (E_{pl} = 100, 150 and 200 kN/mm^2). It will be seen that increasing the modulus of elasticity of the plate increases the bond stresses with a 50 kN/mm^2 change in modulus giving a change in bond stress of 0.7 N/mm^2.

6.6. Effect of the plate width to thickness ratio

Three ratios of plate width to depth were considered; R1 with a plate width of 25 mm, R2 with a width of 50 mm and R3 with a width of 75 mm. In each case, the thickness of the plate was changed to keep the same

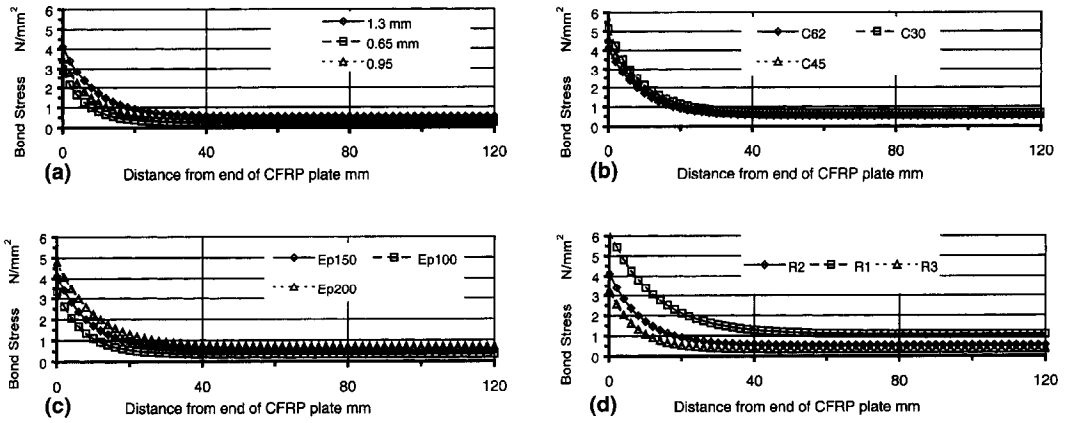

Fig. 9. Results from parameter study: (a) variation in plate thickness; (b) variation in concrete strength; (c) variation in elastic modulus of plate; (d) variation in aspect ratio of plate.

cross section area of the plate. The dimensions of the plates are listed in Table 4.

Fig. 9(d) shows the effect of different plate width to thickness ratios on the interfacial bond stresses. From this figure it can be seen that increasing the ratio of the plate width to the plate thickness b_{pl}/t_{pl} reduces the concentration of bond stress.

6.7. Effect of plate end geometry

The investigation of the plate end geometry included three plate cut-off end shapes as shown in Fig. 10. The three shapes were square (Plan and elevation No:1), tapered plate width (Plan and elevation No:2) and reduced plate thickness (Plan and elevation No:3) ends. The plate thickness, apart from the ends, was kept at 1.3 mm for all cases.

For the reduced plate thickness end, the distance over which the plate thickness was reduced was chosen to cover the expected load transfer distance. This value was taken as 40 t_{pl} and obtained through the consideration

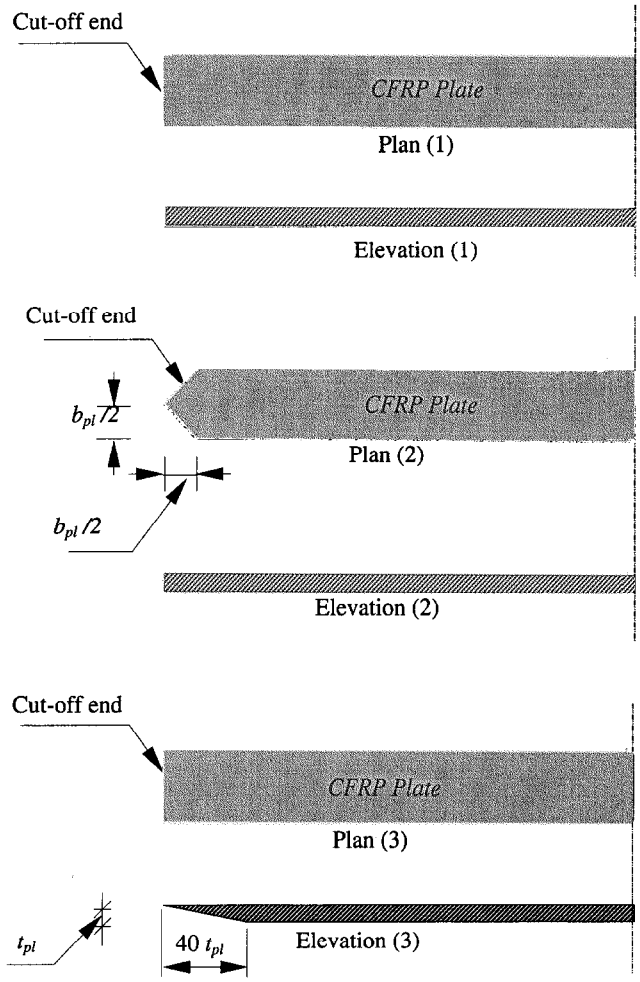

Fig. 10. End details of plates used in parameter study.

Table 4
Plate widths and corresponding thickness for the different b_{pl}/t_{pl} ratios

Notation	Plate width (mm)	Cross-section area of plate (mm^2)	Thickness (mm)	b_{pl}/t_{pl}
R1	25	65	2.6	9.6
R2	50	65	1.3	38.5
R3	75	65	0.87	87.2

of the previous experimental results from the different parameters. This reduction in thickness may not be a very practical procedure, though the same effect could be obtained by layering. It is, nevertheless of interest to establish what the effect would be since, intuitively, it appears to be a means of reducing the high end shears and vertical tensions and hence the peeling effect.

6.8. Calculations of bond stresses for the different plate ends

The calculations of bond stress distribution for the plate with the tapered ends were calculated as follows.

- The width of the plate was divided into strips as shown in Fig. 11. For each strip the bond stress was calculated over the whole length of the plate.
- The bond stress at any position was obtained by superposition of the stresses calculated for each of the individual strips multiplied by its width and the final result divided by the whole width of the section at that position.

For the reduced thickness plate the following procedure was adopted in the calculations.

- The distance within which the change in the thickness of the plate occurred was divided into small increments, 1.5 mm. At each distance measured from the plate end, (1.5 mm, 3.0 mm, 4.5 mm, 6.0 mm, etc. up to the end of the transition zone), the thickness of the plate with reduced thickness ends was calculated.

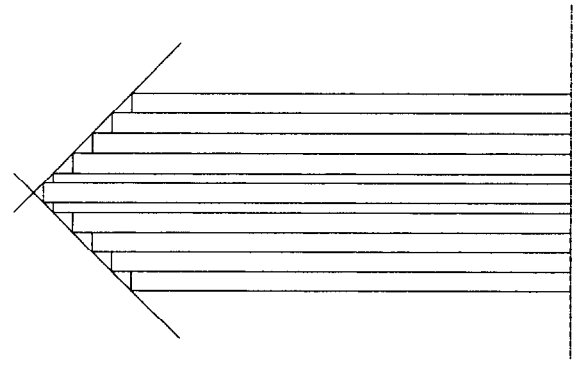

Fig. 11. Idealisation of end of plate with champfered end.

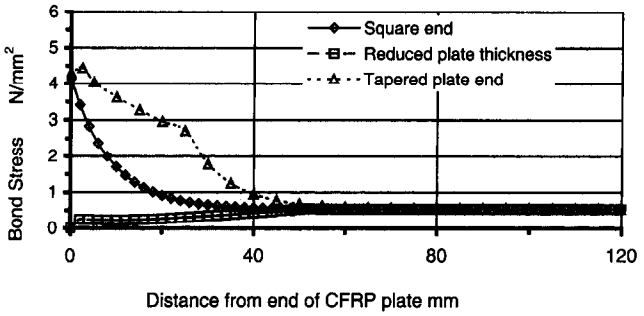

Fig. 12. Influence of different end details on bond stresses.

- These values were used to establish the bond stress for the case of beams bonded with a plate having the calculated depth. The bond stress value at the specific distance from the plate end was considered to represent the bond stress at this point for the reduced thickness plate ends.
- For example, at a distance of 10 mm from the plate end, the plate thickness was 0.25 mm. Then, the proposed model was used to calculate the interfacial bond stress distribution for a beam plated with a plate having square ends with a constant thickness of 0.25 mm. Having established that, only the bond stress value at the specific position under consideration, (10 mm), was taken to represent the bond stress at that position. The method was repeated at small distance increments until the full transition zone was covered. An alternative analysis was carried out using a layered model. This gave a very similar answer.

Fig. 12 shows the effect of the different plate end geometries on the bond stress at the interface. It can be seen that changing the plate end geometry affects the bond stress distribution over the plate. The plate with the tapered end showed nearly same stress value at the plate edge and then the stress reduced gradually until died out at nearly same distance as the square ends plate. However, it should be noted that the bond stress within the load transfer distance was relatively higher compared to the other two geometries.

For the plate with the reduced thickness ends, the bond stress curves have changed dramatically. The bond stress was almost zero at the plate end and started to increase with the increasing distance from the plate end. This increase did not go above the lowest limit of the bond stress for the other two cases of the plate end.

7. Conclusions

For prediction of the stresses in the region of the plate end, the analytical model presented in this paper reasonably represented the trend of the experimental behavior, bearing in mind the average nature of the experimental results. Following the parametric study the conclusions may be summarized as:

- Increasing the plate thickness resulted in higher bond stresses along the interface between the plate and concrete, especially; at the plate ends compared with low thickness plates.
- Increasing the plate thickness resulted in an increase in the load transfer distance, i.e. the distance required for the transition of the forces from the concrete to the plate.
- The ratio of the plate width to the plate thickness b_{pl}/t_{pl} is very significant in defining the bond stresses near the plate ends.
- It can be seen that there was no difference in the bond stresses developed close to the plate ends between the square and tapered plate ends.
- Using a plate with reduced thickness ends resulted in almost zero bond stress at the plate end and started to increase with the increasing distance from the plate end. This increase did not go over the lowest limit of the bond stress for the other two cases of the plate end.
- At the low load levels and within the constant moment region, perfect bond between the plate and the beam was achieved.
- The plate end geometry affects the bond stress at the plate–epoxy–concrete interface, however, more investigation needs to be conducted to clarify the effect of this variable.

References

[1] Etman EEA. Repair and strengthening of reinforced concrete beams using carbon fiber reinforced polymer composite. Ph.D. Thesis, The School of Civil Engineering, The University of Leeds, Leeds LS2 9JT, UK, July 1999. p. 294.

[2] Swamy RN, Jones R, Charif A. Shear adhesion properties of epoxy resin adhesives. In: Sasse, HR, editor. Proceedings of International Symposium on Adhesion between Polymers and Concrete, Aix-en-Provence, 1986, organized by RILEM. London: Chapman & Hall, 1986. p. 741–55.

[3] Ranish EH, Rostasy FS. Bonded steel plates for the reduction of fatigue stress of coupled tendons in multi span bridges. In: Sasse HR, editor. Proceedings of International Symposium on Adhesion between Polymers and Concrete, Aix-en-Provence, 1986, organized by RILEM. London: Chapman & Hall, 1986. p.561–70.

[4] Swamy RN, Jones R, Charif A. The effect of external plate reinforcement on the strengthening of structurally damaged RC beams. Struct Engr 1989;66(3):45–56.

[5] Jones R, Swamy RN, Charif A. Plate separation and anchorage of reinforced concrete beams strengthened by epoxy-bonded steel plates. Struct Engr 1988;66(5):85–94.

[6] Roberts TM. Approximate analysis of shear and normal stress concentration in the adhesive layer of plated RC beams. Struct Engr 1989;67(12):229–33.

[7] Chajes MJ, Finch WW, Januszka TF, Thomson, TA. Bond and force transfer of composite material plates bonded to concrete. ACI Struct J 1996:208–17.
[8] Quantrill RJ, Hollaway LC, Thorne AM. Prediction of maximum plate end stresses of FRP strengthened beams: Part II. Mag Concrete Res 1996;48(177):343–51.
[9] Malek AM, Saadatmanesh H, Ehsani MR. Prediction of failure load of R/C beams strengthened with FRP plate due to stress concentration at the plate end. ACI Struct J 1998:142–52.
[10] Beeby AW, Etman EEA. Repair of reinforced concrete beams with corroded reinforcement using CFRP plates. In: Conference of Structural faults and Repair 99. London, July 1999.